Proceedings of ASME Turbo Expo 2011
GT2011
June 6-10, 2011, Vancouver, British Columbia, Canada

GT2011-46246

EFFECTS OF CO-ROTATING LONGITUDINAL VORTICES ON TURBULENT STRUCTURES IN THE LEG OF THE HORSESHOE VORTEX

Shinji Honami
Tokyo University of Science
Chiyoda-ku, Tokyo, Japan

Masaharu Andoh
Tokyo University of Science
Chiyoda-ku, Tokyo, Japan

Satoshi Tanabe
Tokyo University of Science
Chiyoda-ku, Tokyo, Japan

Masahiro Motosuke
Tokyo University of Science
Chiyoda-ku, Tokyo, Japan

ABSTRACT

Manipulation of the horseshoe vortex is a key technology for improvement of blade performance in the turbine blade passage, since the complicated interaction process of the vortices occurs around the blade. The target of the present study is to clarify the interaction process between the leg vortex of the horseshoe vortex produced by the blade and the longitudinal vortex produced by the vortex generator. The arrangement of the vortex generator wings which correspond to Common Flow Down configuration is discussed. The effect of the spacing of the longitudinal vortices is also tested. The narrow and wide spacing results in the different longitudinal vortex location at the top or side of the horseshoe vortex. The measurement by the hot wire anemometer which has an X-type rotating prong by a stepping motor provides three components of the velocity and the detailed turbulence kinetic energy and the Reynolds stress profiles giving the clear understanding of the complicated interaction process of the two vortices. The narrow spacing of the longitudinal vortex in Common Flow Down configuration shows the strong interaction of the horseshoe vortex and longitudinal vortex dynamics.

INTRODUCTION

The research and development of the turbine blade passage in the aircraft and industrial gas turbine engines have been conducted by the simulation and/or experiment, as shown in Fig. 1 which depicts the research items on the turbine blade passage in the R & D process. The experimental approach is composed of the actual turbine blade test and the element test in the laboratory level such as the cascade wind tunnel test from the view points of aerodynamics, heat transfer and so on. The aerodynamic study is classified into the categories of the primary flow and secondary flow which is thought to be the flow mechanisms induced by the primary flow. Some of the typical examples of the research items on the secondary flow are the horseshoe vortex and its leg vortex interaction, the leakage flow at the blade tip, three dimensional separation at the blade leading edge and the trailing vortex shed from the trailing edge, as shown in Fig. 1.

Understanding of the flow field which composed of the primary flow and secondary flow is the important step for the improvement of blade performance. Control or manipulation of the secondary flow is a key technology in the design process. The primary flow has an essential role on the blade performance. Furthermore, inevitable and important flow mechanism in the turbine blade passage is interaction of the primary flow and the secondary flow such as the leakage flow at the blade tip and the horseshoe vortex at the junction of the blade and end wall. These secondary flows cause flow distortion in the passage and a considerable reduction in the performance compared with the primary flow. Then, the recent studies have focused on prevention and suppression of the strong secondary flow in the passage. In particular, the horseshoe vortex cannot be eliminated by the passive control device[1][2][3], while the suction of the horseshoe vortex can be performed from the view point of active control by Bloxham et al.[4]. They remove the leading edge boundary layer at the cylinder and endwall interface and improved the total pressure

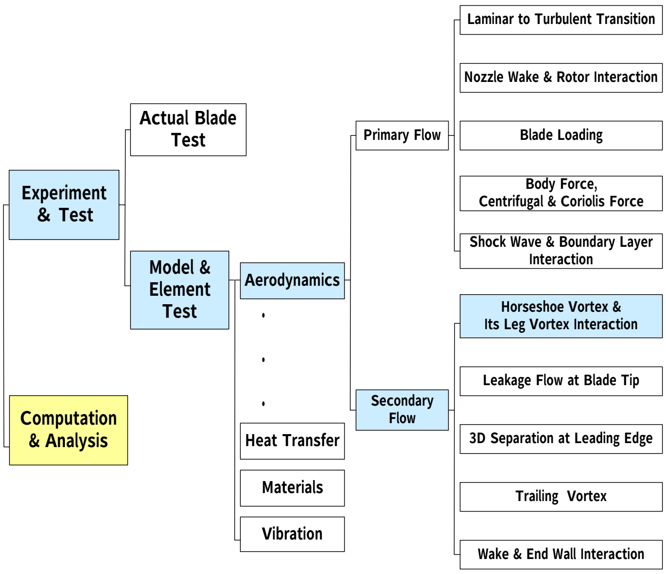

Fig.1 Research and development items in turbine blade

losses by about 30 % with a suction flow rate of 11 % of the approaching boundary layer.

It is also important to understand the turbulence structure produced by the complicated flow mechanism in the turbine blade passage, although it is impossible to measure the turbulence quantities such as the turbulence intensity and the Reynolds normal and shear stresses in the actual passage due to the difficulties in the hot-wire and high speed PIV measurements. Some of the solutions are to utilize the computational approaches including the turbulence model. Other one is to simulate the secondary flow mechanism in the blade passage and to conduct the detailed measurement in a turbine cascade which includes the essential characteristics of the secondary flow mechanisms. In particular, the detailed turbulence quantities are helpful to understand the detailed loss mechanism at the turbulence level[5].

In the previous studies, the interaction process between the horseshoe vortex and the longitudinal vortex has been studied in the different configuration of a pair of vortex generator wings; Common Flow Up[6][7] and Down configuration[8]. Counter-rotating vortices generated by vortex generators are identified by the direction of the secondary flow between them that can be directed either toward or away from the wall. The former is called Common Flow Down, and the latter is called Common Flow Up[9]. The leg vortex of the horseshoe vortex produced by the NACA0024 blade without camber interacted by the longitudinal vortices produced by the vortex generator was discussed in Common Flow Up configuration[6][7]. This case corresponds to the interaction process similar to the behavior of the pressure side leg vortex of the horseshoe vortex interacted with the other leg vortex in the suction side in the actual cascade passage with severe camber as in the flow model[10][11].

It has been also found that the interaction process also occurs in the turbine blade passage which includes the film cooling holes. The cooling jets are injected into the end wall and blade surface boundary layer, resulting in the longitudinal vortices in the boundary layer. Therefore, the wall jet through the inclined hole such as the film cooling hole in the turbine passage might produce the longitudinal vortex such as the vortex generator jet studied by Compton & Johnston [12]. If this longitudinal vortex is interacted with the leg vortex of the horseshoe vortex, the unexpected flow may occur in the actual passage.

The present study depicted by the blue box in Fig.1 is considered to be located at the secondary flow aerodynamics category in the overall research items on the turbine blade passage. The aim of the present study is to clarify the flow field involving the complicated interaction process between the horseshoe vortex and longitudinal vortex in Common Flow Down configuration as a consequence of a series of the previous papers. The objectives are also to show the effect of the co-rotating longitudinal vortex on the turbulence structure of the horseshoe vortex.

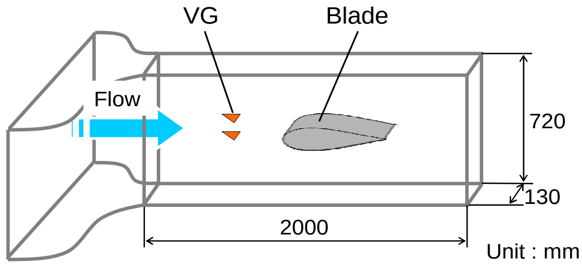

Fig. 2 Wind tunnel

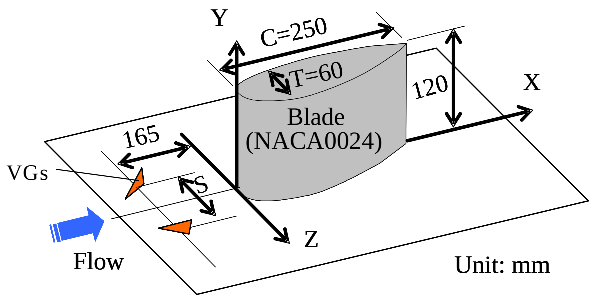

Fig.3 Blade and vortex generator arrangement

EXPERIMENT AND PROCEDURE

Experimental Apparatus

The experiment was carried out in an open wind tunnel as shown in Fig. 2. The test section of the tunnel is 2000 mm long, 720 mm wide and 130 mm high. The reference position is 595 mm upstream from the leading edge of the blade. The reference velocity U_{ref} is 16 m/s, the boundary layer thickness is 20 mm, the momentum thickness is 1.7 mm and the Reynolds number based on the momentum thickness is 1700.

Fig. 3 shows the configuration of vortex generators and the blade. A fixed coordinate system X, Y and Z centered at the intersection of the blade leading edge and the endwall is employed. NACA 0024 with the maximum wing thickness T=60 mm at X/C=0.3, the chord length C=250 mm, radius of curvature of 15.9mm at the leading edge and the span of 120 mm is used as the blade. The angle of attack of the blade is set at zero.

A size and configuration of the vortex generators are decided from the preliminary experiments where the effect of height and spacing of the vortex generator wings on the longitudinal vortex formation is clarified. The wing with height of 15mm has same order of the circulation as that of the horseshoe vortex among three cases of wing height from 10, 15 and 20 mm. The vortex generator shows a linear increase of the vorticity with increasing angle of attack less than 18 deg [11]. Then, the attack angle of the wing is selected at 18 deg. The distance, L, between the blade and vortex generator wings is 11 times as long as the wing height. The distance, L and the spacing of the wings, S, are also determined to arrange the longitudinal vortex at the top or the side of the leg of the horseshoe vortex.

Vortex generators are two half-delta-wings with the height of 15 mm, base of 30 mm and thickness of 1 mm. They are mounted at X=-165 mm. The spacing S between vortex generators is 45 and 110 mm. Common Flow Down configuration is employed in this study as a consequence of a series of the previous papers.

Experimental Procedures

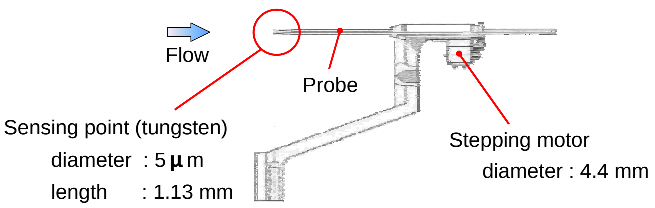

Fig.4 Hot wire with rotating X probe

The rotating X-probe hot-wire anemometer is shown in Fig. 4. This anemometer has an X-type probe with two tungsten wires of 5µm in diameter. The probe can be rotated around X-axis by the minute stepping motor with the diameter of 4.4 mm. The three-components of velocity can be measured by using this anemometer with only one X-probe without the individual probe difference compared with the conventional anemometer which requires the two X-probes. The uncertainty analysis about the rotating X–array hot–wire anemometer estimates to be 3.8 % for mean velocity, and 8.3 % for the Reynolds stresses[13].

Measurement stations for velocity are X=75, 175, 375 and 575mm (X/C=0.3, 0.7, 1.5 and 2.3). In each measurement point, the measurement period is 5 sec and the sampling rate is 5 kHz. After the measurement of U and V components, the hot-wire probe is rotated around X axis, and then the U and W components are measured. The calibrations of the flow angle and velocity are conducted in another wind tunnel with round nozzle of 80 mm in diameter before and after the measurement. The calibration curve of the 5th order polynomial expression on the angle characteristics is obtained by data fitting method.

RESULTS AND DISCUSSIONS

Mean Velocity

Figs. 5 show the contours of streamwise velocity and secondary flow vectors at X/C=0.3 to 2.3 in Common Flow Down configuration. The grey color portion in the figures corresponds to the blade cross section. The reference velocity vector shown at the upper-right corner of the figures represents $0.2U_{ref}$. Coordinates and velocities are normalized by the maximum blade thickness T and the reference velocity U_{ref}, respectively. The left column in Fig. 5 is the baseline case; the velocity distribution of the horseshoe vortex without vortex generators. The center and right columns in Fig. 5 are the velocity distributions in the narrow and wide spacing cases, respectively.

At the measurement stations of X/C=0.3 and 0.7, in the baseline case without vortex generators, the high velocity region near the blade surface is found by the downwash motion of the horseshoe vortex. In the narrow spacing case of S/T=0.75, the high velocity fluid is transferred to the near endwall more remarkably than the baseline case. At the region of $Z/T \geq 1.2$, the low velocity is observed by the upwash motion of the longitudinal vortex. In the wide spacing case of S/T=1.83, there are two local minima. One at Z/T=1.0 is caused by the horseshoe vortex, while the other one located on the right side of the horseshoe vortex corresponds to the longitudinal vortex generated from the vortex generator. The position of horseshoe vortex is not different from the baseline case, but the low velocity region of the horseshoe vortex is decreased, and the horseshoe vortex seems to be pressed against the endwall by the longitudinal vortex. The high velocity fluid is also transferred to the endwall at the right side of the horseshoe vortex by the downwash motion of the longitudinal vortex.

Contours at the further downstream stations of X/C=1.5 and 2.3 are shown in the bottom in Fig. 5. In the baseline case without vortex generators at X/C=1.5, the boundary layer is distorted as in X/C=0. In addition, a merging of the two boundary layers on each side of the blade causes the wake which is almost decayed except the endwall at X/C=2.3. In the narrow spacing case of S/T=0.75, the high velocity region near the blade surface is wider than the baseline case by the downwash motion of the vortex. In addition, the low velocity

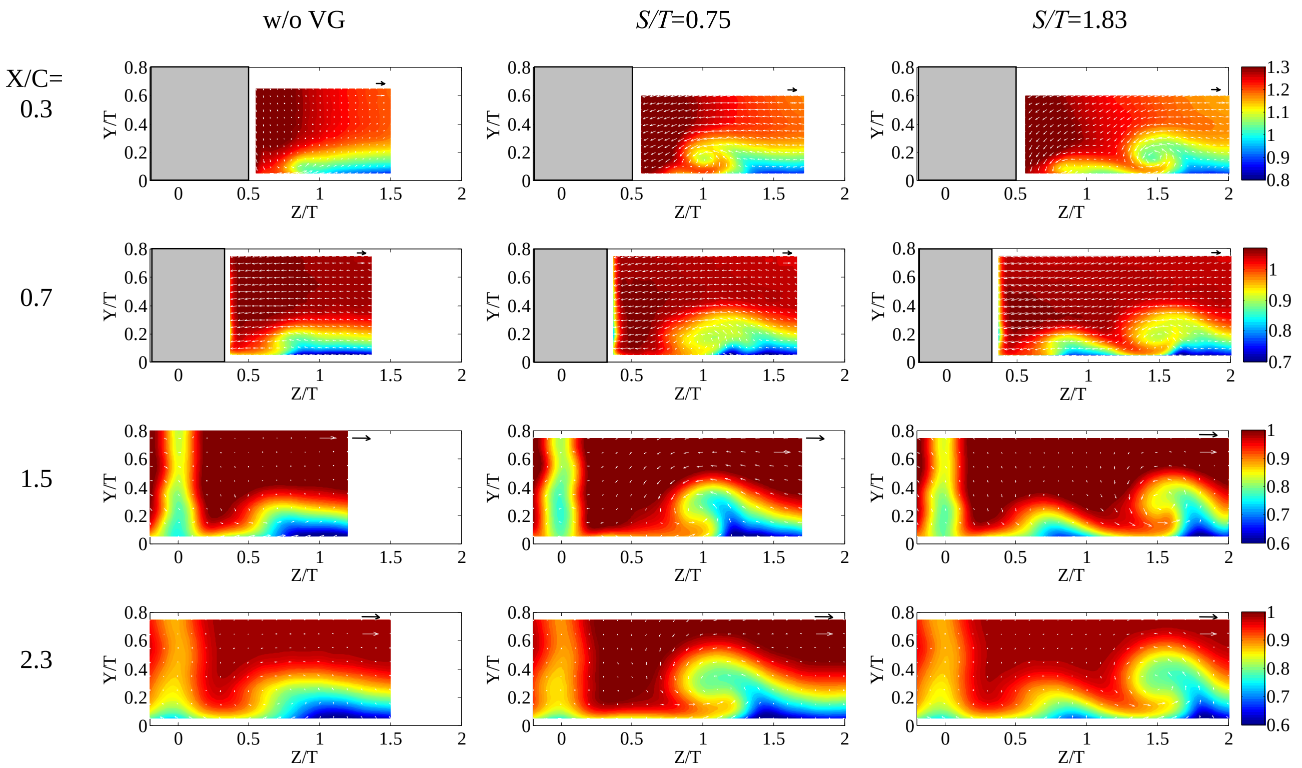

Fig. 5 Contours of streamwise velocity U/U_{ref} (left:baseline, center:narrow, right:wide spacing)

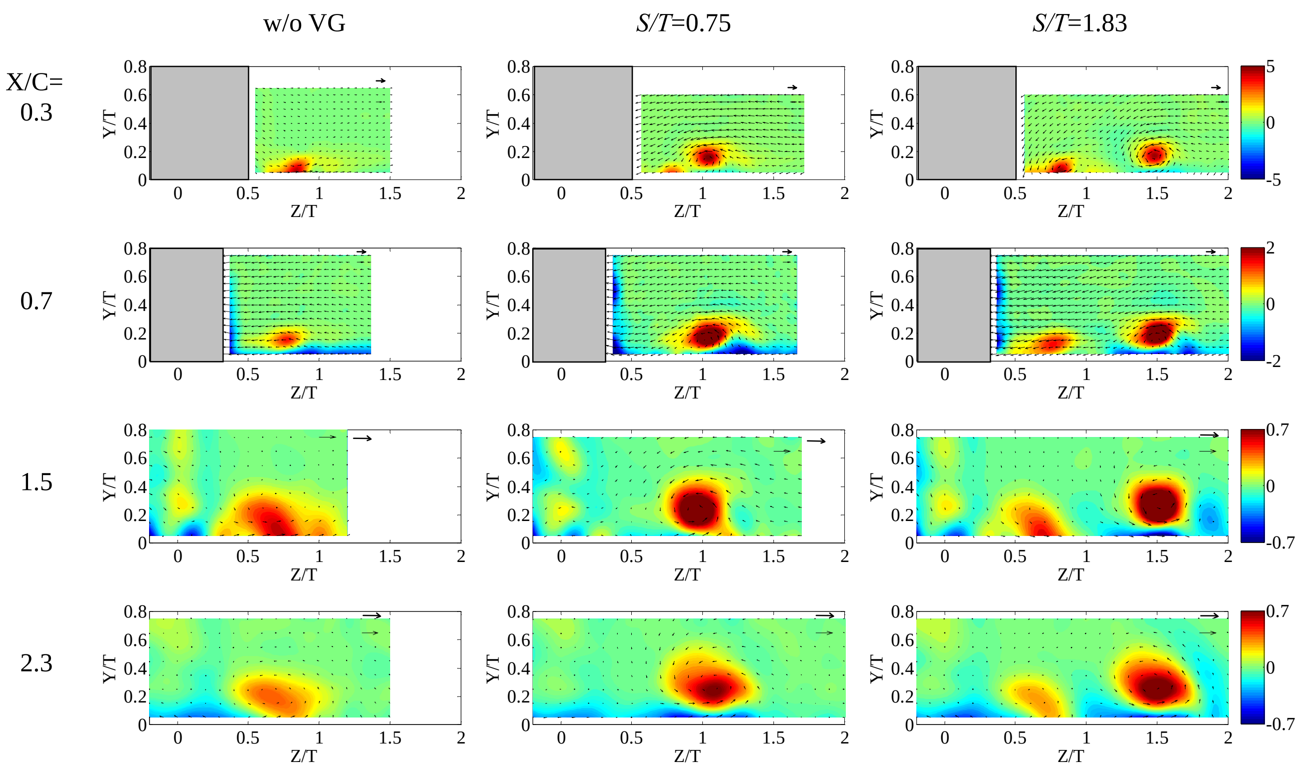

Fig. 6 Contours of streamwise vorticity $\Omega_x T/U_{ref}$ (left:baseline, center:narrow, right:wide spacing)

region spreads at $1.0 \leq Z/T \leq 1.5$ by the upwash motion. In the wide spacing case of *S/T*=1.83, the low velocity region of longitudinal vortex is rolled up by the upwash motion, and the low velocity region of horseshoe vortex becomes smaller.

Vorticity

Figs. 6 show the contours of streamwise vorticity and secondary flow vectors in Common Flow Down configuration. The reference velocity vector and coordinates are the same as those in Figs. 5. The vorticity is normalized by U_{ref} and T.

The transport equation for the stream-wise, x component of the mean vorticity is given by Equation (1).

$$\frac{D}{Dt}\Omega_x = \nu\nabla^2\Omega_x + \left\{\Omega_x\frac{\partial U}{\partial x} + \Omega_y\frac{\partial V}{\partial y} + \Omega_z\frac{\partial W}{\partial z}\right\}$$
$$+\frac{\partial^2}{\partial y\partial z}(\overline{v^2}-\overline{w^2}) + \frac{\partial}{\partial x}\left(\frac{\partial}{\partial z}\overline{uv} - \frac{\partial}{\partial y}\overline{uw}\right) + \left(\frac{\partial^2}{\partial y^2} - \frac{\partial^2}{\partial z^2}\right)(-\overline{vw}) \tag{1}$$

where $\Omega_x, \Omega_y, \Omega_z$ are x, y and z component of the vorticity. The first term in right side is the viscous diffusion, the second one is the vortex stretching by mean strain rate, and the last one is the production due to the anisotropic turbulence structure.

In the baseline case, the horseshoe vortex is located near the endwall. A part of the horseshoe vortex is extended out of the measurement plane at *X/C*=0.3, since the dominant mean strain rate by flow acceleration, $\partial U/\partial x$, increases from the stagnation point of the leading edge to the maximum thickness portion at *X/C*=0.3. Then, the horseshoe vortex seems small in this case at *X/C*=0.3. An elliptical shape of horseshoe vortex can be wholly observed at *X/C*=0.7. The secondary flow toward the blade is observed at *X/C*=0.7, because the blade thickness is thinning, and it causes the negative velocity.

In the narrow spacing case of *S/T*=0.75, there are two local maxima at *X/C*=0.3. One is caused by horseshoe vortex at *Z/T*=0.8. The other one located on the upper-right of the horseshoe vortex is the longitudinal vortex. There might be a possibility that the approaching boundary layer just upstream of the blade is made thin by the downwash motion of the longitudinal vortices in Common Flow Down configuration. This means that the horseshoe vortex seems to have higher vorticity and smaller cross section due to the vortex tube stretching. At *X/C*=0.7, two local maxima are not found, and there is only one strong vortex with an elliptical shape. The horseshoe vortex and the longitudinal vortex seem to be merged. Since the merged vortex is too strong as compared with the horseshoe vortex, it moves in the *Z*-direction by induced velocity of mirror vortex. In the wide spacing case of *S/T*=1.83, the strength of the longitudinal vortex is weaker than the narrow spacing case at *X/C*=0.3. The horseshoe vortex does not move in *Y*-direction, because the vortex is pressed against the endwall by the longitudinal vortex.

Contours at *X/C*=1.5 and 2.3 are shown in the bottom of Fig. 6. In the baseline case, there are local maxima in the vorticity. The large one at *Z/T*=0.7 is the horseshoe vortex. The other small one located at *Z/T*=0.3 seems to be a trailing vortex from the blade trailing edge. At *X/C*=2.3, there is a large elliptical shape vortex. In this region, there is only one local maximum in the vorticity, because the horseshoe vortex merges with the trailing vortex. In the narrow spacing case, the trailing vortex is not found. And there is a strong round shape vortex. The negative vorticity is generated under the merged vortex near the endwall. In the wide spacing case, the horseshoe vortex becomes weaker and smaller compared with the baseline case. It is considered that the upwash motion by the horseshoe vortex and the downwash one by the longitudinal vortex are interacted at the boundary of the two vortices with each other and this interaction attenuates the vorticity of the horseshoe vortex.

In conclusion, the strength of the horseshoe vortex is affected by interaction with the longitudinal vortex as well as the mean strain rate by the stream-wise flow acceleration and deceleration, $\partial U/\partial x$.

Turbulence Profiles

Figs. 7(a), (b) and (c) show the contours of the Reynolds normal and shear stresses and turbulence kinetic energy in the baseline case, the narrow spacing case and the wide spacing case in Common Flow Down configuration.

The production terms of Reynolds normal stress in the transport equation are given by Equation (2).

$$\frac{1}{2}\overline{u^2} : -\overline{u^2}\frac{\partial U}{\partial x} - \overline{uv}\frac{\partial U}{\partial y} - \overline{uw}\frac{\partial U}{\partial z} \tag{2.a}$$
$$\frac{1}{2}\overline{v^2} : -\overline{uv}\frac{\partial V}{\partial x} - \overline{v^2}\frac{\partial V}{\partial y} - \overline{vw}\frac{\partial V}{\partial z} \tag{2.b}$$
$$\frac{1}{2}\overline{w^2} : -\overline{uw}\frac{\partial W}{\partial x} - \overline{vw}\frac{\partial W}{\partial y} - \overline{w^2}\frac{\partial W}{\partial z} \tag{2.c}$$

The production terms of Reynolds shear stress in the transport equation are given by Equation (3).

$$-\overline{uv} : \overline{u^2}\frac{\partial V}{\partial x} + \overline{v^2}\frac{\partial U}{\partial y} - \overline{uv}\frac{\partial W}{\partial z} + \overline{uw}\frac{\partial V}{\partial z} + \overline{vw}\frac{\partial U}{\partial z} \tag{3.a}$$
$$-\overline{uw} : \overline{u^2}\frac{\partial W}{\partial x} + \overline{w^2}\frac{\partial U}{\partial z} + \overline{uv}\frac{\partial W}{\partial y} - \overline{uw}\frac{\partial V}{\partial y} + \overline{vw}\frac{\partial U}{\partial y} \tag{3.b}$$
$$-\overline{vw} : \overline{v^2}\frac{\partial W}{\partial y} + \overline{w^2}\frac{\partial W}{\partial z} + \overline{uv}\frac{\partial W}{\partial x} + \overline{uw}\frac{\partial V}{\partial x} - \overline{vw}\frac{\partial U}{\partial x} \tag{3.c}$$

In Fig. 7(a), the higher level of the Reynolds normal stress of $\overline{u^2}$ is observed at the low velocity region of the horseshoe vortex, while the low level of $\overline{u^2}$ is found at high velocity region caused by the downwash motion of the horseshoe vortex downstream of the blade at *X/C*=1.5 and 2.3. High $\overline{v^2}$ and $\overline{w^2}$ is observed at the vortex boundary due to the strong vortex motion associated with a large scale of vortex structure. The profile of Reynolds shear stress, $-\overline{uv}$ shows a peak value at the vortex center in the upstream station which is similar pattern from that of the vorticity as in Fig. 6 and at the vortex boundary in the downstream station. The profile of $-\overline{uw}$ also corresponds to the strong shear layer on the blade surface at *X/C*=0.7 and in the wake at *X/C*=1.5 and 2.3. Then, the severe total pressure loss in the horseshoe vortex is attributed to the higher turbulence level through the production and dissipation process of the turbulence energy.

In Fig. 7(b), the Reynolds normal stresses, $\overline{u^2}$, $\overline{v^2}$ and $\overline{w^2}$ show an interesting profile which has a local maximum

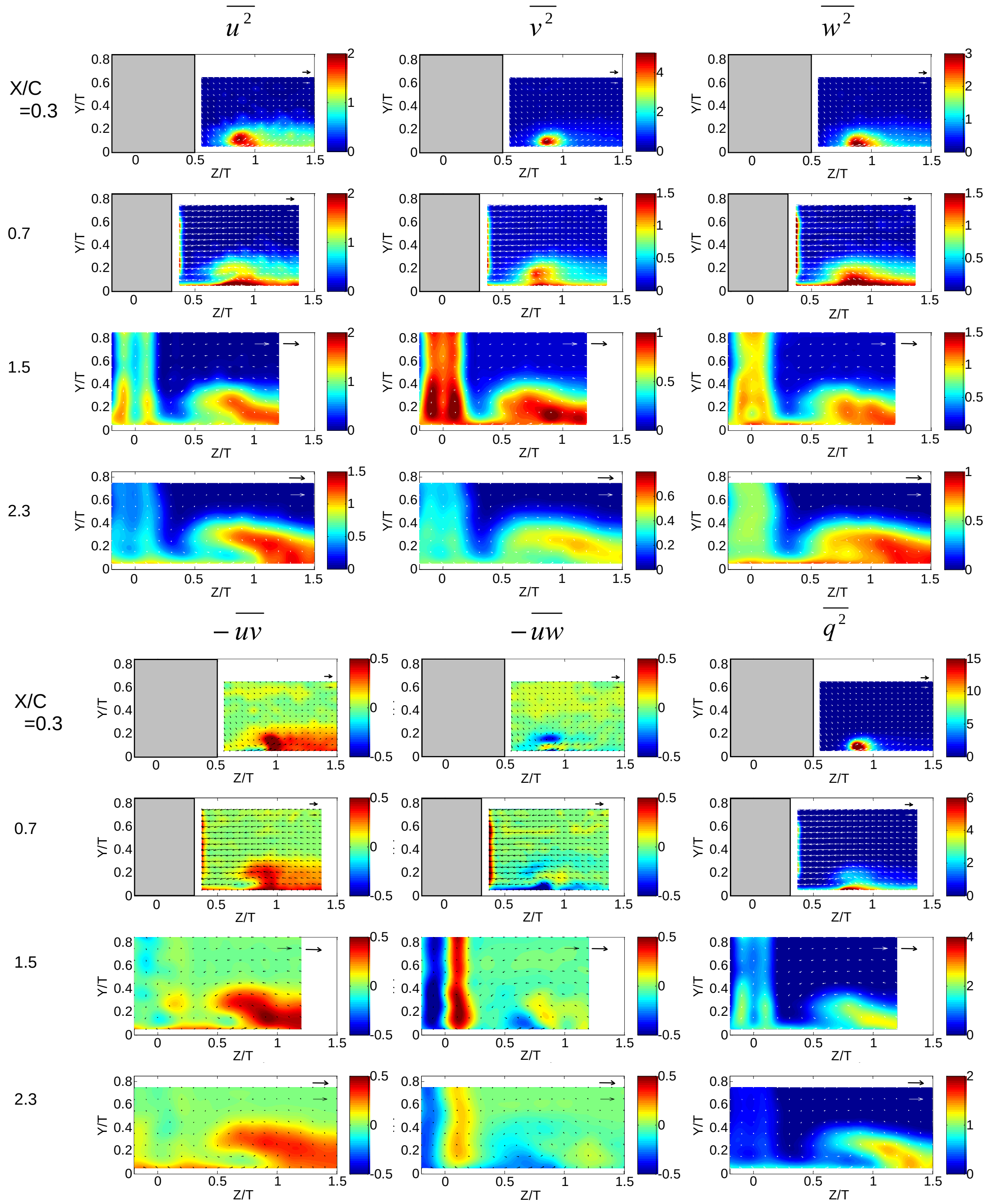

Fig.7(a) Reynolds normal & shear stress and turbulence kinetic energy, baseline case without vortex generators around the vortex. Then, it is found that the vortex shape is clear at X/C=1.5 and 2.3. The Reynolds shear stress, $-\overline{uv}$ shows a positive and negative value at the top and bottom of the horseshoe vortex, while the Reynolds shear stress, $-\overline{uw}$ shows a positive and negative value at the right and left side of the vortex at the downstream station. It is explained by the way in which the mean strain rates increases at the boundary of the horseshoe vortex and on the blade surface as shown in Equations (2) and (3), respectively.

In Fig. 7(c), a very similar pattern to that of the baseline

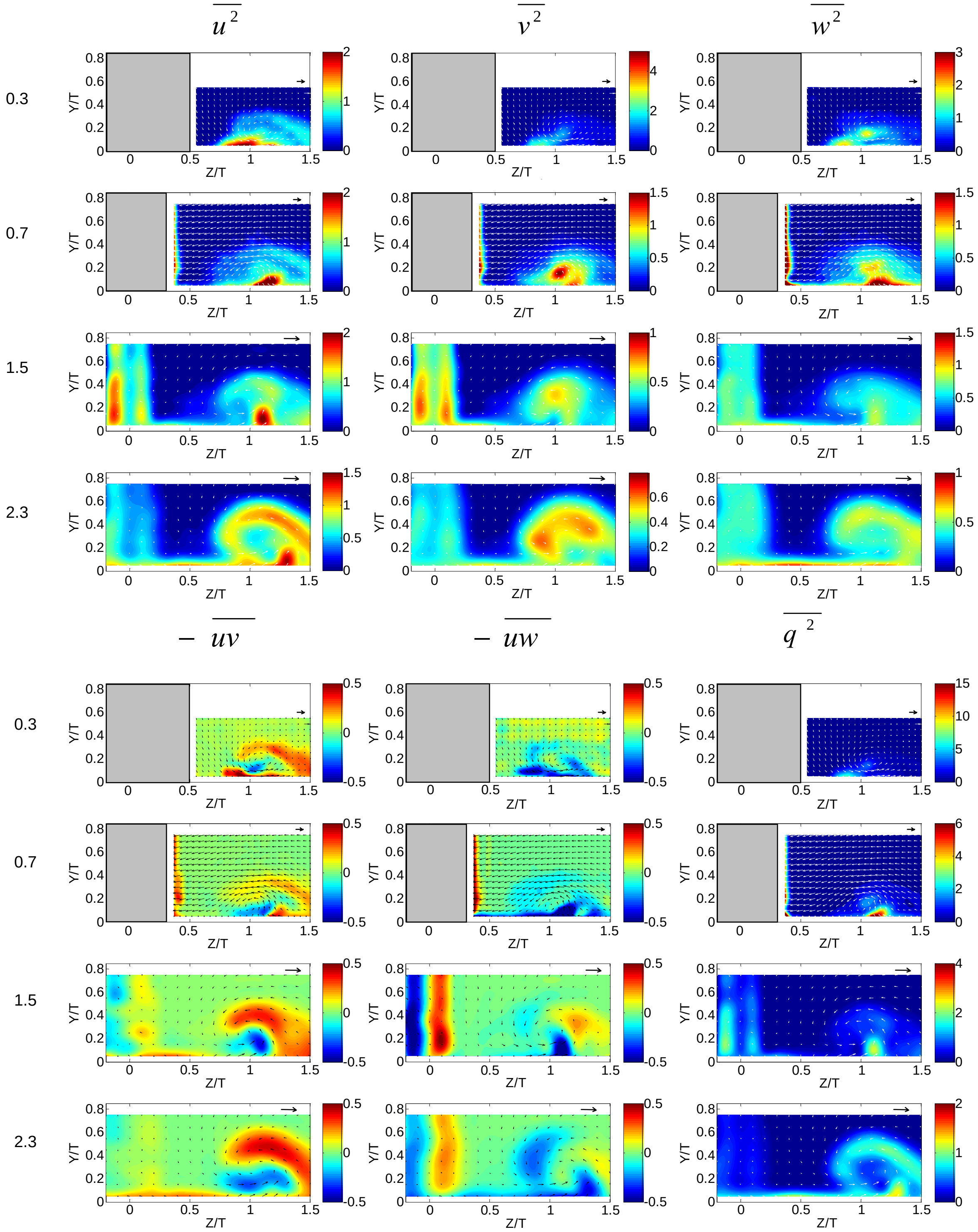

Fig.7(b) Reynolds normal & shear stress and turbulence kinetic energy, Narrow spacing, S/T=0.75

case is observed with the Reynolds normal and shear stresses, although the horseshoe vortex is attenuated by the longitudinal vortex interaction.

Total Pressure Loss

Fig. 8 shows contours of total pressure loss at different angle of the vortex generators, ϕ which corresponds to the total pressure difference between reference and local position normalized by the dynamic pressure at the reference station.

Fig. 9 also shows the area-averaged total pressure loss coefficient, λ at *X/C*=1.5. A broken line represents total pressure loss coefficient in the baseline case without the vortex generators.

In the narrow spacing case of *S/T*=0.75, the total pressure loss coefficient is not sensitive to the angle of attack of vortex generator wings in the range of $0<\phi<7.2$. The high pressure region grows by the downwash motion and the migration from the blade surface of the merged vortex at ϕ =7.2 in Fig. 8. At ϕ >10.8, an increase in the total pressure loss is attributed to the loss by the vortex generators and the longitudinal vortex. Both losses are increased with the increase in ϕ.

In the wide spacing case of *S/T*=1.83, λ shows lower value in the range of $0<\phi<7.2$ compared with that of ϕ =0. The tendency of λ at ϕ >10.8 is increased similarly as in the narrow spacing case, but, the rate of increase in the wide spacing case is higher. In the narrow spacing of the longitudinal vortices, the boundary layer thickness at the leading-edge of the blade becomes thin by strengthened downwash motion of the longitudinal vortices. Then, the strength of the longitudinal vortex and the horseshoe vortex changes with the increase in ϕ. In contrast, in the wide spacing of the longitudinal vortices, the vortex pair does not contribute mostly to formation of the horseshoe vortex. As a result, the loss of the horseshoe vortex remains constant, and the increasing of the loss of the longitudinal vortex affects directly the total pressure loss. Although the vortex generators introduce the total pressure loss, they have much effect on the interaction process between the leg vortex and longitudinal vortex depending on the spacing and angle of attack of upstream vortex generators.

It is worth denoting that the overall profiles with the total pressure loss, the time averaged velocity and turbulent Reynolds stresses are helpful for understanding the detailed loss mechanism in the horseshoe vortex in the complicated interaction process with the longitudinal vortex. The high level of the Reynolds stress in the horseshoe and longitudinal vortices due to the production mechanism by the strong mean strain rate in the mean velocity field results in the total pressure loss through the dissipation process of the turbulence kinetic energy. The new knowledge and understanding on the flow mechanism by the different category approaches as shown in Fig. 1 could be fed back to the performance improvement of the turbine passage.

CONCLUSIONS

An experimental investigation of vortices produced by upstream vortex generators and the two legs of the horseshoe vortex formed at the leading edge of a straight blade was performed by means of a rotating hot wire anemometry in a low-speed wind tunnel. The legs of the horseshoe vortex are also affected by the interaction of the vortices produced by different configuration. The detailed time mean and turbulence velocity profiles show useful information on the total pressure loss mechanism through the turbulence kinetic energy production process. The following conclusions are obtained.

(1) The horseshoe vortex is merged with the co-rotating longitudinal vortex located at the top of the horseshoe vortex in narrow spacing case, while it is not merged with the longitudinal vortex located at the side of the horseshoe vortex in wide spacing case.

(2) In narrow spacing case, the Reynolds normal stresses, $\overline{u^2}$, $\overline{v^2}$ and $\overline{w^2}$ have a local maximum around the vortex. The Reynolds shear stress, $-\overline{uv}$ and $-\overline{uw}$ show a positive and negative value at the top and bottom and at the right and left side of the vortex, respectively.

(3) In wide spacing case, the Reynolds normal and shear stresses show a very similar pattern from that of the baseline case.

NOMENCLATURE

C = chord length (=250mm)
L = distance between blade and VG wings (=165mm)
$\overline{q^2}$ = turbulence kinetic energy
S = spacing of vortex generators (=45 & 110mm)
T = maximum blade thickness (=60mm)
U, V, W = time-averaged velocity components in X, Y and Z directions
$\overline{u^2}$, $\overline{v^2}$ and $\overline{w^2}$ = Reynolds normal stress
$-\overline{uv}$, $-\overline{uw}$ = Reynolds shear stress
U_{ref} = reference velocity
X, Y, Z = streamwise, vertical, spanwise directions
ϕ = angle of attack of vortex generator wing
λ = area averaged total pressure loss coefficient
Ω_x = time-averaged streamwise vorticity

REFERENCES

[1] Kubendran, L. R., McMahon, H. M. & Hubbarttte, J. E., 1986, Turbulent Flow Around a Wing / Fuselage Type Juncture, *AIAA J.*, Vol.24, No.9, pp.1447-1452

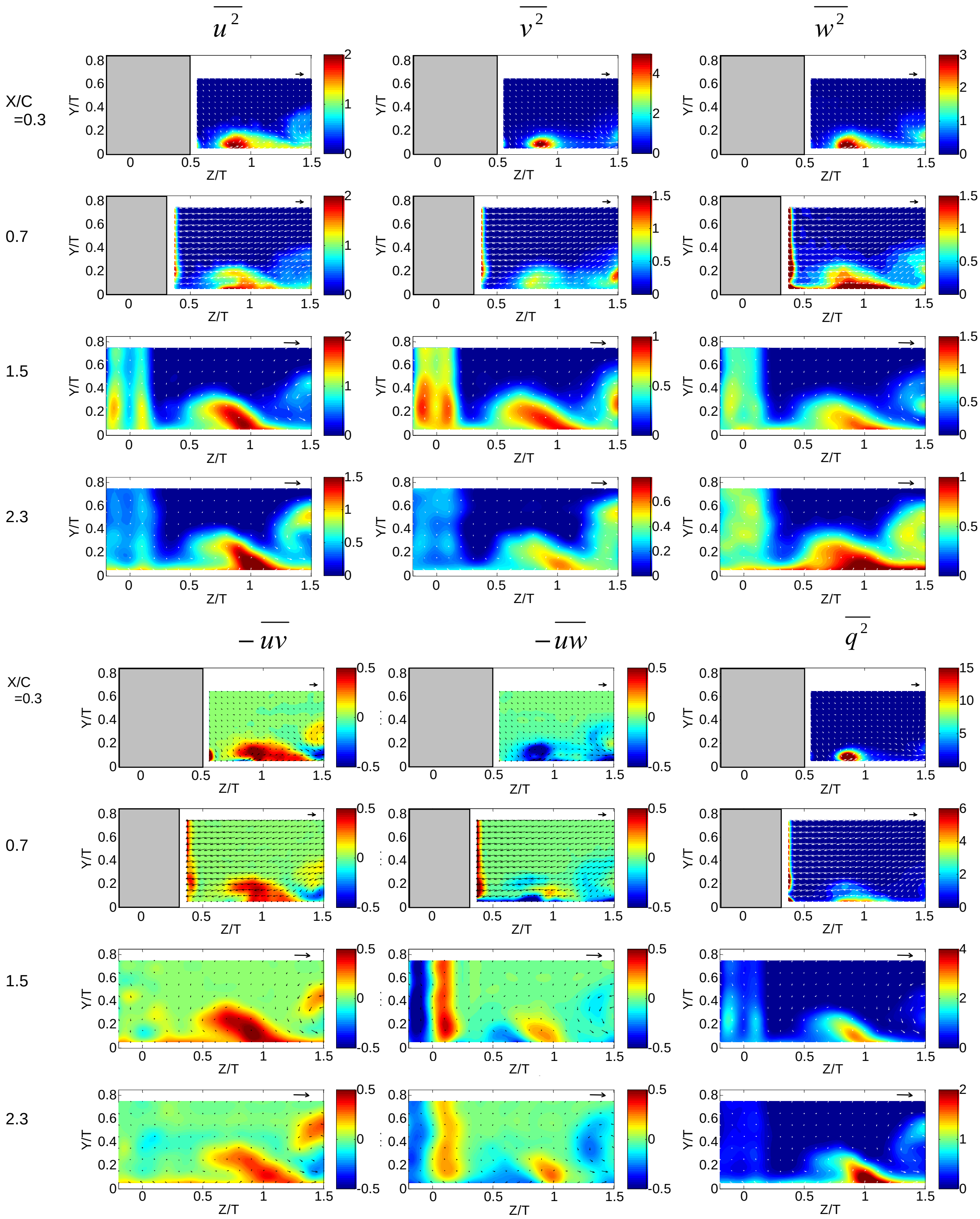

Fig. 7(c) Reynolds normal & shear stress and turbulence kinetic energy, Wide spacing, *S/T*=1.83

[2] Devenport, W. J., Dewitz, M.R., Agarwal, N.K., Simpson, R.L. & Poddaret, K., 1990, Effects of a Fillet on the Flow Past a Wing-Body Junction, *AIAA J.*, Vol.28, No.12, pp.2017-2024

[3] Mahmood, G. I., Gustafson, R. & Acharya, S., 2005, Experimental Investigation of Flow Structure and Nusselt Number in a Low-Speed Linear Blade Passage With and Without Leading-Edge Fillets, *ASME J. Heat Transfer*,

127, pp.499-512.

[4] Bloxham, M., Hollisii, R. & Bons, J., 2008, Horseshoe Vortex Control with Leading Edge Endwall Boundary Layer Removal, *AIAA* 2008-4319.

[5] Gregory-Smith, D.G. et al, 1988, Turbulence Measurements and Secondary Flows in a Turbine Rotor Cascade, *ASME J., Turbomachinery*, Vol.110,pp 479-485.

[6] Andoh, M., Motosuke, M. & Honami, S., 2009, Interaction of Longitudinal Vortex with Horseshoe Vortex~ Configuration -Effect of Longitudinal Vortex-, AIAA Fluid Dynamic Conference, *AIAA*-2009-4176, San Antonio

[7] Andoh, M., Motosuke, M., & Honami, S., 2010, “Interaction Between Horseshoe Vortex and Longitudinal Vortices From the Vortex Generators,” ASME Turbo Expo 2010, *ASME GT*2010-23222, Glasgow

[8] Tanabe, S., Andoh, M., Motosuke, M., & Honami, S., 2010, “Effect of Interaction between Horseshoe Vortex and Co-rotating Longitudinal Vortices with Different Configuration” Proc Third Int. Conf. on Jets, Wakes and Separated Flows, *ICJWSF*-2010, Cincinnati, Ohio

[9] Pauley, W. R. & Eaton, J. K., 1988, Experimental Study of the Development of Longitudinal Vortex Pairs Embedded in a Turbulent Boundary Layer, *AIAA J.*, Vol.26, No.7, pp.816-823

[10]Langston, L. S., 1980, Crossflows in a Turbine Cascade Passage, *ASME J. Eng. Power*, 102, pp. 866–874.

[11] Sharma, O. P. & Butler, T. L., 1983, An experimental investigation of the three-dimensional unsteady flow in an axial flow turbine, *AIAA* 83-1170

[12]Compton,D.A. & Johnston,J.P., 1992, Streamwise vortex production by pitched and skewed jets in a turbulent boundary layer, *AIAA J*,30, pp640-647

[13]Shizawa, T. & Mizusaki, Y., 2004, Response of Time-Depended Flowfield Structure Behind an Active Vortex Generators Pair, *AIAA* Paper 2004-0427

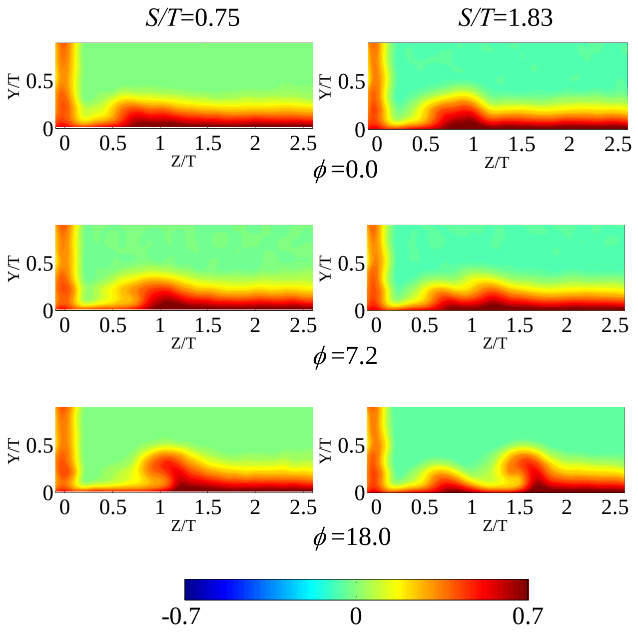

Fig. 8 Contours of total pressure loss

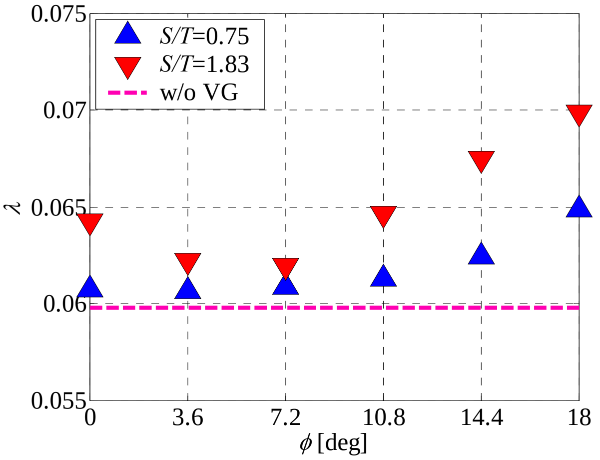

Fig. 9 Total pressure loss coefficient λ vs. angle of attack of vortex generator wing, ϕ